INSTITUTE OF PHYSICS PUBLISHING SUPERCONDUCTOR SCIENCE AND TECHNOLOGY

Supercond. Sci. Technol. **16** (2003) 1554–1558 PII: S0953-2048(03)67086-7

Effects of the superconductivity transition on the response of YBCO edge transition bolometers

Ali Bozbey[1,2], **M Fardmanesh**[1], **I N Askerzade**[3], **M Banzet**[4] **and J Schubert**[4]

[1] Electronics Engineering Department, Bilkent University, Ankara 06533, Turkey
[2] Department of Physics, Faculty of Sciences, Ankara University, 06100-Ankara, Turkey
[3] Institute of Physics, Azerbaijan National Academy of Sciences, H Cavid-33, Baku-370143, Azerbaijan
[4] ISG, Research Center Juelich (FZJ), D52425 Juelich, Germany

E-mail: fardman@ee.bilkent.edu.tr

Received 4 August 2003, in final form 24 September 2003
Published 13 November 2003
Online at stacks.iop.org/SUST/16/1554

Abstract

Dependence of the phase and magnitude of the response of Y–Ba–Cu–O edge transition bolometers on the superconducting transition is studied. The responses of both large and small area devices were investigated and several anomalies are observed. The response of small area $LaAlO_3$ devices considerably differed from that expected based on the dR/dT curve. This discrepancy is observed to be strongly dependent on the superconducting transition. Both the phase and magnitude/(dR/dT) of the response of the devices showed abrupt changes for below the $T_{c\text{-onset}}$ when measured versus temperature, while the phase variation also showed strong dependence on the modulation frequency. We present the analysis and propose mechanisms responsible for the modulation frequency dependence of the response characteristics versus temperature, within the superconductivity transition region of the devices.

1. Introduction

There have been several studies investigating the temperature dependence of the lattice properties [1–3], optical properties [4, 5] and, thermal properties [6–13] of $YBa_2Cu_3O_{7-x}$ and YBCO/substrate boundary resistance [14–16]. In these studies, some anomalies through the superconductivity transition have been reported. The reported anomalies were mostly minor and the investigations involving optical response have not been based on the phase and magnitude of the response separately, rather on the time constant of the device, which comprises both components and is less sensitive to the device parameters. We have investigated the change in the thermal parameters and the heat propagation–radiation absorption mechanism by investigating both the phase and the magnitude of YBCO edge transition bolometers (ETB) on crystalline $LaAlO_3$ and MgO substrates. Both large area patterns and small area patterns were analysed.

The responsivity versus modulation frequency and temperature has previously been analysed and according to the simple RC model it follows [16–18]:

$$r = \left(\frac{\eta I}{G(1 + j\omega\tau)}\right)\frac{dR}{dT} \tag{1}$$

where $\tau = C/G$, I is the dc bias current, η is the absorption coefficient, ω is the modulation frequency, r is the responsivity and C and G are the total thermal conductance and thermal capacitance of the bolometer, respectively. From equation (1), the phase of the response can be obtained from

$$\tan\theta = -\frac{\omega C}{G}. \tag{2}$$

There have already been reports on the modulation frequency dependence of the response of the bolometers based on the classical bolometer modelling for strong and weak thermal coupling conditions [13, 19, 21]. Dwir *et al* investigate both small area and large area bolometers' response magnitudes under modulation frequencies up to 50 kHz and wavelength range of $\lambda \sim$ 600–4500 nm, and also report wavelength independent performance for both types of devices [19]. Fardmanesh *et al* have already analysed the deviation of

Table 1. Physical properties of the measured devices on 1 mm thick $LaAlO_3$ substrate. In this paper only the measurements from devices on chips 1 and 3 are reported. The results of the devices on chip 2 are the same as chip 1.

Device number	Device name	Chip number	ΔT (K)	Pattern type	Pattern area (mm^2)	Patterning technique	Substrate material
1	First type small area device	1	2	Microbridge	0.001	Ion beam etching	$LaAlO_3$
2	Second type small area device	1	2	Microbridge	0.002	Ion beam etching	$LaAlO_3$
3	First type small area device	2	3.8	Spiral	0.01	Ion beam etching	$LaAlO_3$
4	Second type small area device	2	3.9	Spiral	0.02	Ion beam etching	$LaAlO_3$
5	Large area device	3	2.9	Spiral	1.7	Chemical	$LaAlO_3$

the phase and magnitude of the response versus temperature from that based on the classical bolometer modelling for low modulation frequencies [13]. Here we present the analysis to explain the observed changes in the phase and the thermal parameters in the devices at the superconducting transition, for frequencies up to 100 kHz. We associate these changes with the change in the energy or the angle of the incident phonons on to the substrate boundaries reaching out from the film as the temperature is varied.

2. Samples and experimental setup

The samples studied in this paper were made of typically 200 nm thick YBCO films on 0.5–1 mm thick substrates, deposited by magnetron sputtering or pulsed laser deposition techniques [24]. The devices were patterned to either microbridge (1–12 μm) or spiral (5 or 50 μm wide) designs [12, 24]. The micro bridges and 5 μm spirals resulted in 0.001–0.002 mm^2 pattern areas and 50 μm wide spirals resulted in 1.7 mm^2 pattern areas. For the contact pads of the YBCO patterns, we deposited ∼50 nm thick gold after pre-etching YBCO for approximately 5 nm. For this purpose we used Denton Vacuum Desk II etch-sputter unit. We used silver epoxy for the wire contacts.

According to their pattern areas (A) and response behaviours, we classified the samples used in this paper as the first and second type small area bolometers on $LaAlO_3$ substrate ($A \cong 0.002$ mm^2), large area bolometers on $LaAlO_3$ substrate ($A \cong 1.7$ mm^2) and small area bolometers on MgO substrate ($A \cong 0.002$ mm^2). The first and second type small area bolometers are on the same substrate and separated from each other with less than 0.5 mm distance. The reasons for different characteristics are not completely understood and the classification can be done only after the measurements. The details of the samples and the measurement results are presented in section III and table 1 is provided for comparing the physical properties of the devices. In this paper, only the measurements for the $LaAlO_3$ substrate based devices are presented since the measurements for the MgO based devices have already been presented in [12, 13]. This is while the analysis done for the $LaAlO_3$ devices showed to be valid for the MgO substrate based devices as well.

The responses of the samples were measured using a dc bias current, I_{bias}, in 4-probe configuration using an automated low-noise characterization setup. The temperature of the substrate was controlled with maximum 20 mK deviation from the target temperature with liquid nitrogen based dewar and a software PID controller. For the temperature sweep measurements, 1 K min^{-1} heating–cooling rate was used minimizing the temperature gradient between the sensor and the sample. Similar holder configuration and contacts were used as in [12]. The phase and magnitude of the devices were measured with SR 850 DSP lock-in amplifier, the input of which was amplified with an ultra-low noise preamplifier (Stanford SR 570). As a radiation source, electrically modulated, fibre coupled IR laser diode with wavelength of 850 nm, and 12 mW power was used. Since the quartz window was not close enough to the sample, we used a lens to focus the light to get higher intensity without sacrificing from the homogeneity of the light on the patterns. In all of the measurements, the signal-to-noise ratio was above 100. The resistances of the devices were measured simultaneously with the phase and magnitude of the response so that one can see any deviation of the magnitude of the response from dR/dT. The small area results reported in this paper are obtained from a single substrate and both of them were measured without changing the experimental environment in order to get the same substrate/cold–head thermal resistance, R_{sc}.

3. Results and discussion

The magnitude and phase of the response of the samples were measured versus temperature, T, at the normal to superconductor transition from above $T_{c\text{-onset}}$ to about $T_{c\text{-zero}}$. The main phase [13] and magnitude [13, 19] characteristics of the response of the bolometers have already been reported at the normal to superconductivity transition. Dwir *et al* report deviations of the magnitude of the response from the dR/dT curve and associate it with the used high bias current of 10 mA, smoothening the response curve relative to dR/dT curve measured at 10 μA. However, our previous dc characterization studies demonstrate that as the bias current increases, the normal to superconductor transition curve gets sharper till the instability criterion is reached due to the excessive Joule heating [20]. Our optical response and resistance measurements are done simultaneously for eliminating any error associated with any possible temperature shift due to Joule heating and/or other temperature shift from that measured by the temperature sensor. Here the phase and magnitude behaviour of the response of large area and small

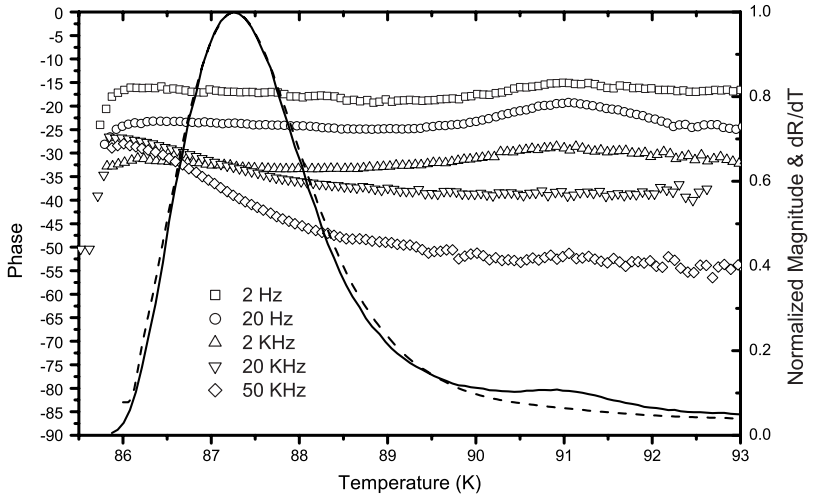

Figure 1. The temperature dependence of the phase (scatter plots) and magnitude (solid line) of the IR response and $\mathrm{d}R/\mathrm{d}T$ (dash line) of large area bolometer on $LaAlO_3$ substrate.

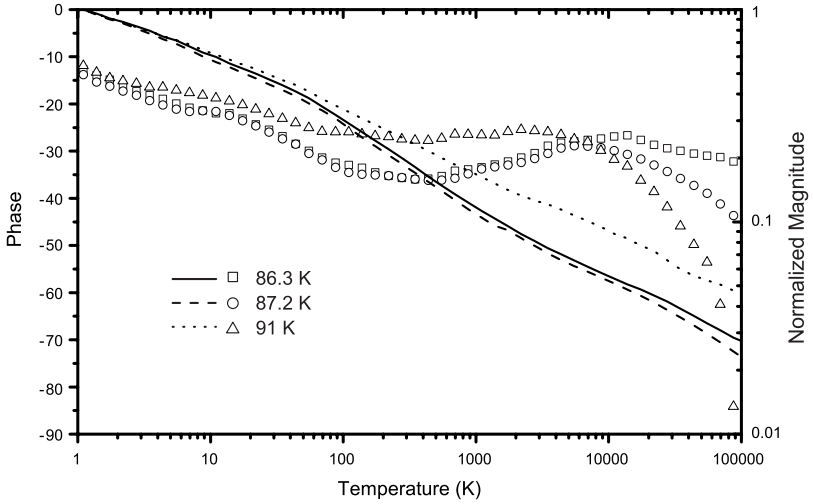

Figure 2. The phase (scatter plots) and magnitude (solid line) of the IR response versus frequency measured at temperatures $T_{\text{c-zero}}$, T_{c} and $T_{\text{c-onset}}$ for large area bolometer on $LaAlO_3$.

area devices are analysed separately as they are found to have two distinct behavioural characteristics.

3.1. Measured response characteristics versus T and f_m

3.1.1. Large area devices. As shown in figure 1, the magnitude of the response follows the $\mathrm{d}R/\mathrm{d}T$ curve very closely for a large area device. But there are distinct behaviours for the phase of the response at low and high modulation frequencies as shown in the corresponding response versus frequency plot in figure 2 [12, 13].

The response of our large area devices is well measured to be limited by the substrate/cold–head thermal boundary conductance, G_{sc}, at low modulation frequency, f_m, where the thermal diffusion length into the substrate is higher than the substrate thickness, t_s. The response at the mid-range frequencies is mainly limited by the substrate heat capacitance, C_s, and thermal conductance, G_s, determined by the thermal diffusion length, $L_f = (D/\pi f)^{1/2}$, where $D = k_s/C_s$ is the thermal diffusivity of the substrate material [11]. In the relatively high f_m range, e.g. 10 kHz, L_f is less than 50 μm for $LaAlO_3$ substrate devices [25]. That is, the thermal variations at the surface effectively diffuse about 50 μm below the film before damping away. Thus, the film/substrate thermal conductance, G_{fs}, and film capacitance, C_f in this frequency range become comparable to G_s and C_s respectively [12, 15, 26] and dominate in the response of the devices.

3.1.2. Small area devices. Our small area $LaAlO_3$ substrate devices are found to be much more sensitive to variation of the thermal parameters at the superconducting transition compared to all devices on MgO substrate and large area devices on $LaAlO_3$. We found a particular behavioural variation in the phase of the response, which was dependent on both the bridge and small spiral patterns on the same substrate.

In all the devices, the response magnitude/($\mathrm{d}R/\mathrm{d}T \times$ bias current) decreased as we go to lower temperatures independent of the modulation frequency as shown in figure 3. The measured absorbtivity of our devices did not show any considerable abrupt change around T_{c} similar to that reported in [4]. Thus, according to the basic RC model, having I, η, ω

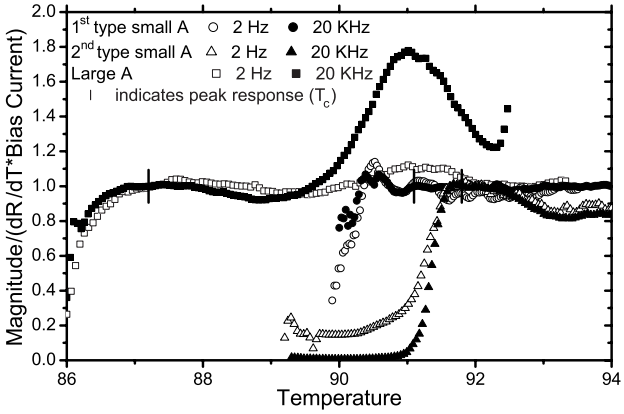

Figure 3. Magnitude of the response normalized with respect to the derivative of the resistance and the bias current for large area and small area bolometers on $LaAlO_3$.

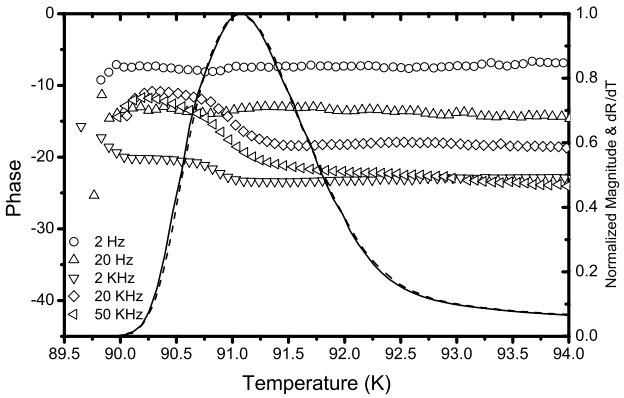

Figure 4. The temperature dependence of the phase (scatter plots) and magnitude (solid line) of the IR response and dR/dT (dashed line) of first type small area bolometer on $LaAlO_3$ substrate.

constant, the change of phase and magnitude is interpreted to be due to the change of total C and/or G of the devices.

Separate analysis for the low frequency and high frequency ranges was made since the effective thermal parameters in the response differ from each other as mentioned above.

3.2. Low frequency response analysis

In the low frequency range the most dominant parameter is the substrate/cold–head thermal boundary resistance, R_{sc}. As shown in figures 1 and 4, the phase response of the small area $LaAlO_3$ substrate devices differs from that of the large area devices. In the large area devices, we observed approximately 20% more phase lag, i.e. slower response, associated with their relatively higher total thermal capacitance. The low-frequency IR response of large area devices was analysed and presented elsewhere previously [13]. There was concluded that the transition-dependent change of the phase of the response is due to the effects of the order parameter of the YBCO material on the phonon spectrum, which determines the Kapitza boundary resistance.

The devices of figures 5 and 6 (first and second type small area bolometers) are on the same substrate and separated from each other with less than 0.5 mm distance. At

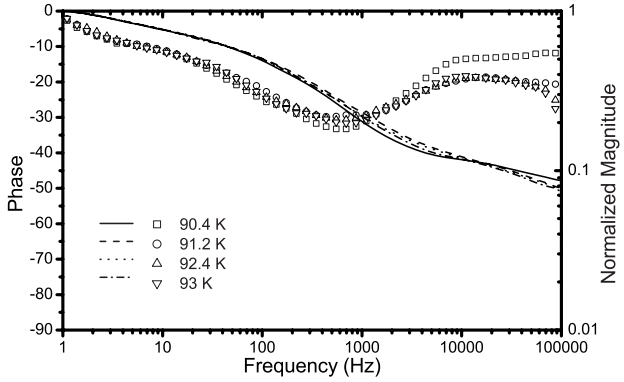

Figure 5. The phase (scatter plots) and the magnitude (solid line) of the IR response versus frequency measured at temperatures around T_c, $T_{c\text{-zero}}$ and $T_{c\text{-onset}}$ for first type small area bolometer on $LaAlO_3$.

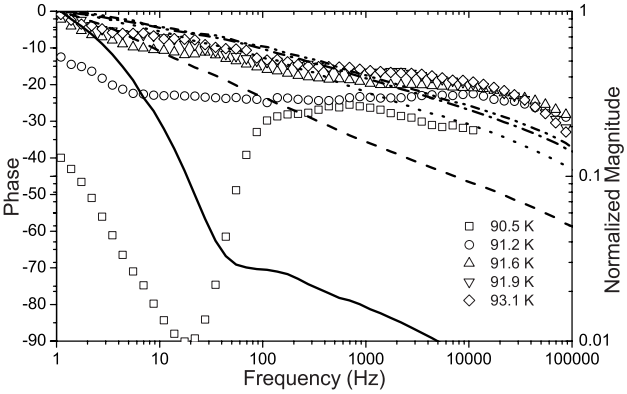

Figure 6. The phase (scatter plots) and the magnitude (solid line) of the IR response versus frequency measured at temperatures around T_c, $T_{c\text{-zero}}$ and $T_{c\text{-onset}}$ for second type small area bolometer on $LaAlO_3$.

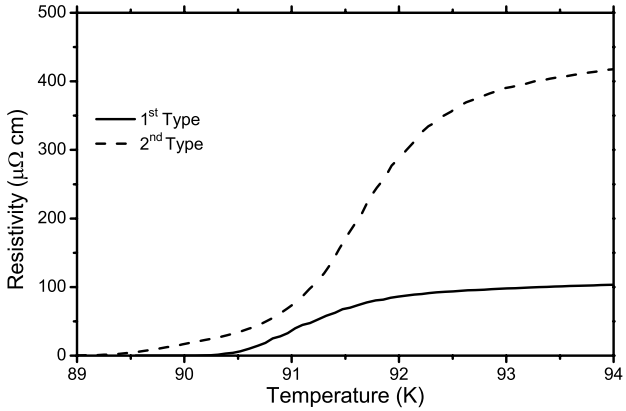

Figure 7. Resistivities of first and second type small area bolometers on $LaAlO_3$ substrate for demonstrating the correlation between the resistivity and the optical response of the devices. (See figures 5 and 6.)

second type bolometers, in the low-frequency range, where the thermal diffusion length is comparable to the substrate thickness, and R_{bd} can be neglected compared to R_s or R_{sc}, we observed phase deeps around the knee frequencies as shown in figure 6. As seen in figure 7, the resistivity of second type small area bolometer is much higher than that of the first type

which might be correlated to possible high *ab*-plane electrical and thermal resistivity. There have been studies reporting on such correlation using the Wiedemann–Franz law which addresses the electrical and thermal resistivities of metals with the relation $k(T) = L \times \sigma(T) \times T$ where L is the Lorenz number, k and σ are the thermal and electrical conductances of the material respectively [27, 28]. Our ongoing thermal modelling results agree with the above-suggested correlation. Thus, we associate the observed phase deep with low *ab*-plane thermal conductance and the strong dependence of response to the heat capacitance of the device, which is more dominant with devices with lower G according to equation (1).

3.3. High frequency response analysis

In the high frequency range the dominant parameters are C_s, R_s, C_f and R_{fs}, due to short L_f. R_{sc} is not effective anymore since the heat waves cannot reach the cold-head boundary. The phase difference at the same f_m between the large area devices and small area devices increases as f_m gets closer to the frequency range where C_f starts to dominate. Thus, this is associated with the relative sizes of the thermal capacitances of two devices which are proportional to the film areas. The phase lag of all our devices at high f_m decreased at lower temperatures, as shown in figures 1 and 4. This can also be observed from the phase versus modulation frequency curves in the range of about 10–100 kHz in figures 2 and 5. However, the phase versus frequency behaviour differs in small area devices, compared to that of the large area devices especially in the high-end frequency range. As shown in figures 4 and 5 for $f_m > 10$ kHz, the phase of the first type small area device starts to increase with increasing frequency at $T_{\text{c-zero}}$ while the phase of the large area device keeps the same trend at $T_{\text{c-onset}}$ as also shown in figures 1 and 2. We observed this increase of phase with increasing frequency for a number of devices some of which had an increase more than that shown in figure 5.

In all the devices, increase of phase by lowering T, independently of the pattern, suggests an increase in the thermal conductance and/or a decrease in the film or substrate capacitance [15] for both large and small area patterns.

In the large area patterns, G parameter is found to be more dominant in determining the behaviour of the phase. The magnitude versus f_m for the large area pattern of figure 1 is also shown in figure 2, which suggests a decrease in the G_{fs}. Based on the thermal acoustic mismatch theory, this can be explained by the change in the energy or the angle of the incident phonons reaching the film/substrate boundary [13]. The change of the energy of the phonons might be associated with the increase of the superconductor parameter, 2Δ, at temperatures closer to $T_{\text{c-zero}}$ [13]. In small area patterns, the film/substrate thermal conductance and substrate thermal conductance are lower compared to that of the large area devices. Thus C_f and C_s are expected to have more dominant effects especially at higher frequencies ($j\omega C$ terms in electrical analogs). Thus, in this range we associate the further decrease of the phase lag in small area devices with the decrease of total heat capacity of the device.

4. Conclusion

The response of large and small area devices versus temperature and frequency were investigated. The large area devices showed systematic behaviour as expected from the classical bolometric modelling. However, the small area $LaAlO_3$ substrate devices have shown two basic types of behaviours. We associate this with the fact that the devices whose sizes are smaller compared to the substrate thickness (e.g. devices 1 and 2 on chip 1 in table 1) are more sensitive to all the involved thermal parameters than the devices with sizes in the range of substrate thickness (e.g. device 5 on chip 3 in table 1) which could also explain the mixed observed behaviours or anomalies such as the phase deep around the knee frequency or the increase in phase at lower temperatures with increasing f_m at higher frequency end. This was observed only in our $LaAlO_3$ substrate devices and is associated to be due to its lower thermal conductivity compared to that of MgO substrate devices. Having a wide range of the characteristics of the bolometers based on their designs and the materials, a general thermal model is under development to cover all the observed characteristics leading to engineering optimizations of different kinds of superconducting bolometers.

Acknowledgments

The author AB would like to thank Tolga Kartaloglu and Gurkan Figen for their help in the preparation of the measurement setup.

References

[1] Skelton E F *et al* 1989 *Phys. Rev.* B **39** 2779–80
[2] You H *et al* 1988 *Phys. Rev.* B **38** 9213–6
[3] Srinivasan R *et al* 1988 *Phys. Rev.* B **38** 889–92
[4] Yagil Y *et al* 1995 *Phys. Rev.* B **52** 15582–91
[5] Zhang Z *et al* 1992 *J. Heat Transfer* **114** 644–52
[6] Inderhees S E *et al* 1987 *Phys. Rev.* B **36** 2401–3
[7] Taillefer L *et al* 1997 *Phys. Rev. Lett.* **79** 483–6
[8] Williams R K *et al* 1998 *Phys. Rev.* B **57** 10923–88
[9] Cohn J L *et al* 1992 *Phys. Rev.* B **45** 13144–7
[10] Villard C *et al* 1996 *Phys. Rev. Lett.* **77** 3913–6
[11] Fardmanesh M *et al* 1995 *J. Appl. Phys.* **77** 4568–75
[12] Fardmanesh M 2001 *Appl. Opt.* **40** 1080–8
[13] Fardmanesh M and Askerzade I N 2003 *Supercond. Sci. Technol.* **16** 28–32
[14] Shi L *et al* 1993 *Phys. Rev.* B **48** 6550–5
[15] Robbes D *et al* 1999 *IEEE Trans. Appl. Supercond.* **9** 3874–7
[16] Nahum M *et al* 1991 *Appl. Phys. Lett.* **59** 2034–6
[17] Kraus H 1996 *Supercond. Sci. Technol.* **9** 827–42
[18] Richards P L 1988 *Appl. Phys. Lett.* **54** 283–5
[19] Dwir B and Pavuna D 1991 *J. Appl. Phys.* **72** 3855–61
[20] Fardmanesh M *et al* 1998 *IEEE Trans. Appl. Supercond.* **8** 69–78
[21] Depond J-M *et al* 1994 *Physica* C **235–240** 3387–8
[22] Harrabi K *et al* 2000 *Supercond. Sci. Technol.* **13** 1222–6
[23] Sergeev A V *et al* 1994 *Phys. Rev.* B **49** 9091–6
[24] Schubert J *et al* 2000 *Appl. Surface Sci.* **168** 208–14
[25] Fardmanesh M *et al* 1999 *Appl. Opt.* **38** 4735–42
[26] Prasher R S and Phelan P E 1997 *J. Supercond.* **10** 473–84
[27] Takenaka K *et al* 1997 *Phys. Rev.* B **56** 5654–61
[28] Zhang Y *et al* 2000 *Phys. Rev. Lett.* **84** 2219–22